ESTIMATION OF FOREGROUNDS IN WIDE-FIELD MEASUREMENTS OF REDSHIFTED 21 CM POWER SPECTRA WITH THE HYDROGEN EPOCH OF REIONIZATION ARRAY

Nithyanandan Thyagarajan[1*], TBD
Draft version December 9, 2015

ABSTRACT

Keywords: cosmology: observations — dark ages, reionization, first stars — large-scale structure of universe — methods: statistical — radio continuum: galaxies — techniques: interferometric

1. INTRODUCTION

The period in the history of the Universe characterized by the transition of neutral hydrogen in the intergalactic medium (IGM) to a fully ionized state due to the formation of radiating objects such as the first stars and galaxies is referred to as the Epoch of Reionization (EoR). This is an important period of nonlinear growth of matter density perturbations and astrophysical evolution leading to the large scale structure observed currently in the Universe. And yet, this period in the Universe's history has remained poorly probed to date with observations.

The redshifted neutral hydrogen from the IGM in this epoch has been identified to be one of the most promising and direct probes of the EoR (Sunyaev & Zeldovich 1972; Scott & Rees 1990; Madau et al. 1997; Tozzi et al. 2000; Iliev et al. 2002). Numerous experiments using low frequency radio telescopes targeting the redshifted 21 cm line from the spin-flip transition of H I have become operational such as the Murchison Widefield Array (MWA; Lonsdale et al. 2009; Bowman et al. 2013; Tingay et al. 2013), the Precision Array for Probing the Epoch of Reionization (PAPER; Parsons et al. 2010), the Low Frequency Array (LOFAR; van Haarlem et al. 2013) and the Giant Metrewave Radio Telescope EoR experiment (GMRT; Paciga et al. 2013). These instruments have sufficient sensitivity for a statistical detection of the EoR signal via estimating the spatial power spectrum of the redshifted H I temperature fluctuations (Beardsley et al. 2013; Thyagarajan et al. 2013). These instruments are intended to be precursors and pathfinders to the next generation of low frequency radio observatories such as the Hydrogen Epoch of Reionization Array[3] (HERA; DeBoer et al. 2015) and the Square Kilometre Array[4] (SKA). These next-generation instruments will advance the capability from a mere statistical detection of the signal to a direct three-dimensional tomographic imaging of the H I during the EoR.

The most significant challenge to low frequency EoR observations arises from the extremely bright Galactic and extragalactic foreground synchrotron emission which are $\sim 10^4$ times stronger than the desired EoR signal (Di Matteo et al. 2002; Ali et al. 2008; Bernardi et al. 2009, 2010; Ghosh et al. 2012). All the current and future instruments rely on the inherent differences in spatial isotropy and spectral smoothness between the EoR signal and the foregrounds to extract the EoR power spectrum (see, e.g., Furlanetto & Briggs 2004; Morales & Hewitt 2004; Zaldarriaga et al. 2004; Santos et al. 2005; Furlanetto et al. 2006; McQuinn et al. 2006; Morales et al. 2006; Wang et al. 2006; Gleser et al. 2008).

When expressed in the coordinate system of power spectrum measurements described by the three-dimensional wavenumber (k), the foreground emission is restricted to a wedge-shaped region commonly referred to as the *foreground wedge* (Bowman et al. 2009; Liu et al. 2009, 2014a,b; Datta et al. 2010; Liu & Tegmark 2011; Ghosh et al. 2012; Morales et al. 2012; Parsons et al. 2012; Trott et al. 2012; Vedantham et al. 2012; Dillon et al. 2013; Pober et al. 2013; Thyagarajan et al. 2013; Dillon et al. 2014) whereas the EoR signal has spherical symmetry due to its isotropy which appears elongated along line of sight k modes due to peculiar velocity effects when dominated by matter density perturbations during early stages of reionization. The extreme dynamic range required to subtract foregrounds precisely demands high precision modeling of foregrounds as observed by modern wide-field instruments (Thyagarajan et al. 2015b,a).

2. DELAY SPECTRUM

(Parsons et al. 2012)

3. THE WIDE-FIELD "PITCHFORK" EFFECT

(Thyagarajan et al. 2015b,a)

4. SIMULATIONS

We describe the instrument and foreground models used in our simulations.

4.1. *The Hydrogen Epoch of Reionization Array*

4.1.1. *Antenna Power Pattern*

(Neben et al. 2015)

4.1.2. *Antenna Reflectometry*

Patra et al. 2015 (submitted), Ewall-Wice et al. 2015 (submitted)

4.2. *Foreground Model*

5. ANALYSIS OF FOREGROUND SIGNATURES

Figure 1 shows the simulated visibilities from foregrounds, the redshifted H I fluctuations, and residual

[1] Arizona State University, School of Earth and Space Exploration, Tempe, AZ 85287, USA
[*] e-mail: t_nithyanandan@asu.edu
[3] http://reionization.org/
[4] https://www.skatelescope.org/

foregrounds visibilities after deconvolution along the delay axis. The black curves indicate visibilities obtained with an achromatic antenna power pattern (does not change with frequency over the entire bandwidth) while the gray curves are the corresponding visibilities for a chromatic beam. The solid lines in black and gray denote foreground visibilities. The dashed curves in the same colors denote visibilities from simulated redshifted H I fluctuations, and the dotted-dashed lines denote the residual visibilities obtained after deconvolution of the foreground delay spectra. The orange curve denotes a wideband Blackman-Harris window applied to the foreground visibilities to produce delay spectra which were subsequently deconvolved to obtain the residual visibilities. The red, blue and green curves denote the narrowband Blackman-Harris window weights centered on 150, 160 and 170 MHz each of effective bandwidth $\simeq 10$ MHz that will be applied to the simulated EoR H I signal and the foregrounds (both simulated and residual visibilities).
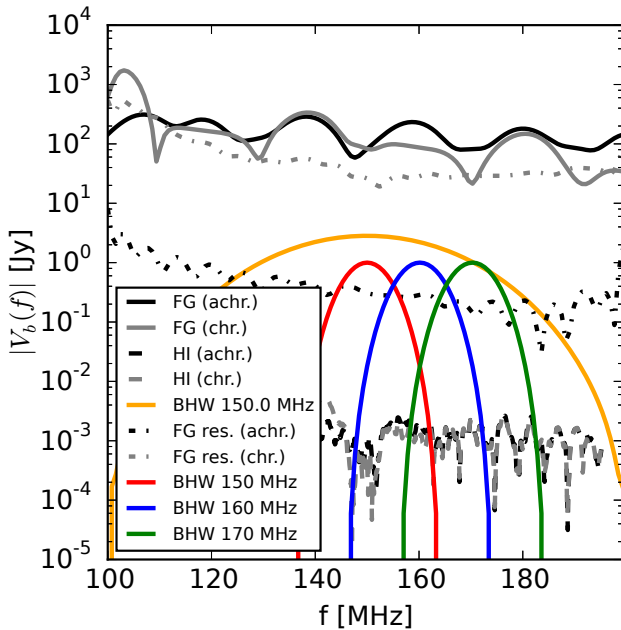

Figure 1. Simulated EoR H I and foreground visibilities over 100 MHz bandwidth for a 14.6 m baseline of HERA.

Figure 2 shows the delay spectra of simulated foreground visibilities (in orange) obtained with chromatic (dashed) and achromatic (solid) beams both weighted with the wideband Blackman-Harris window functions in the spectrum, the corresponding CLEAN components in gray and the residuals in black. The depth of deconvolution is set by the limit at which the rms of the residuals inside the horizon limits becomes equal to that on the outside. It is observed that the visibilities simulated with chromatic power pattern (dashed orange) are significantly broadened in delay spectra due to the additional chromaticity. The delay deconvolution is restricted to the *foreground wedge* with three additional delay bins on either side of the wedge. Due to this restriction, the residuals inside the horizon delay limits are lower than those outside. Since the simulated visibilities obtained using the achromatic power pattern are predominantly contained well within the horizon delay lim-

its, the delay-domain deconvolution of these delay spectra is much more effective at lowering the residuals (by ~ 2 orders of magnitude) than in the case of visibilities obtained with a chromatic power pattern. These delay spectrum residuals correspond to the visibility residuals plotted in Figure 1.
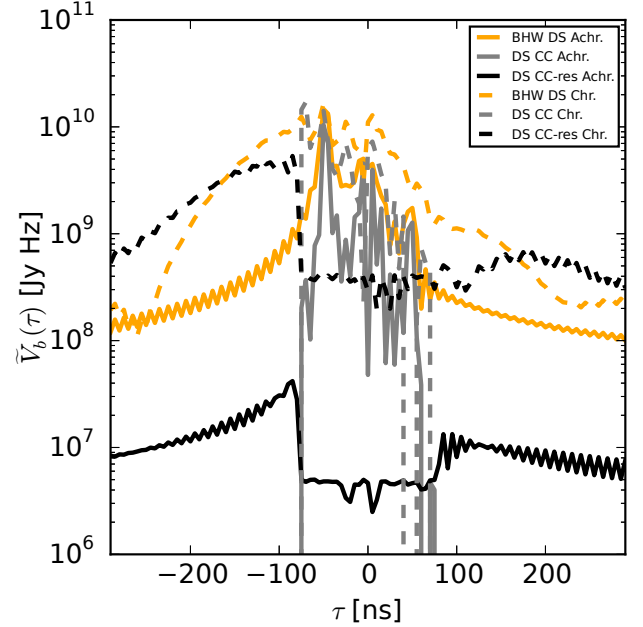

Figure 2. .

Figure 3 shows the delay spectra of the simulated EoR H I fluctuations and the foregrounds. The three panels show the three different center frequencies (150, 160, and 170 MHz) around which the delay spectra were obtained using the narrow band Blackman-Harris window functions shown earlier in Figure 1. Delay spectra obtained using chromatic and achromatic antenna power patterns are shown in black and gray colors respectively. The dashed lines denote delay spectra of foreground residuals obtained after complex delay-domain deconvolution under the concept of foreground removal. The dotted lines denote the foreground delay spectra obtained under the concept of foreground avoidance where foregrounds were not removed but simply down-weighted by the narrowband Blackman-Harris window unctions.

It is noticed from Figure 1 that the foregrounds are about 5 orders of magnitude brighter than the EoR H I fluctuations in the visibilities. From Figure 3 it is seen that the foreground visibilities under foreground avoidance and their residuals under foreground removal are still brighter than the EoR signal. The delay spectra of foreground residuals however are much closer in magnitude to the EoR signal (to a factor $\lesssim 10$) at $|\tau| \gtrsim 200$ ns.

6. SUMMARY
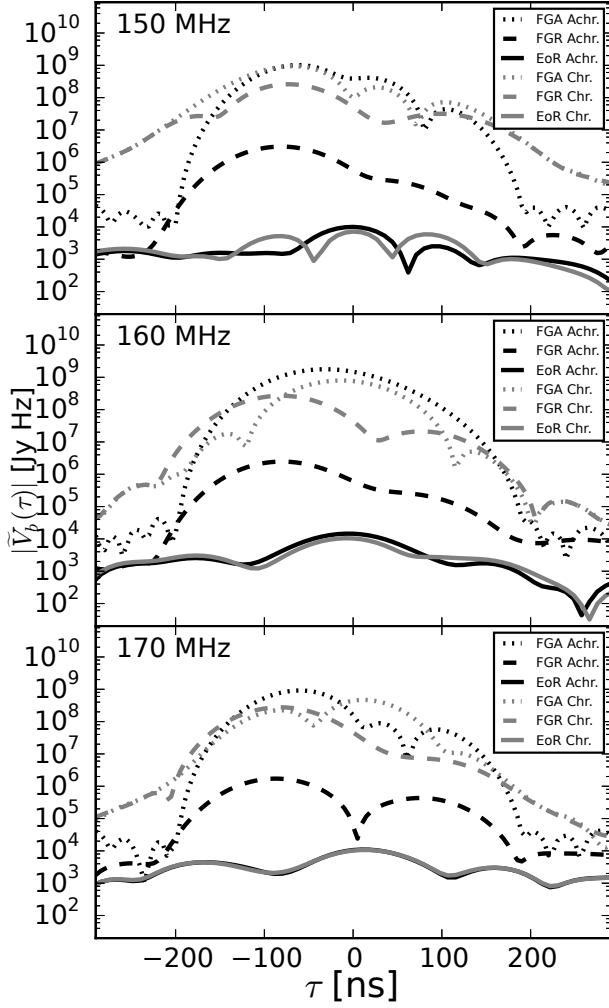
Figure 3. .

REFERENCES

Ali, S. S., Bharadwaj, S., & Chengalur, J. N. 2008, MNRAS, 385, 2166

Beardsley, A. P., Hazelton, B. J., Morales, M. F., et al. 2013, MNRAS, 429, L5

Bernardi, G., de Bruyn, A. G., Brentjens, M. A., et al. 2009, A&A, 500, 965

Bernardi, G., de Bruyn, A. G., Harker, G., et al. 2010, A&A, 522, A67

Bowman, J. D., Morales, M. F., & Hewitt, J. N. 2009, ApJ, 695, 183

Bowman, J. D., Cairns, I., Kaplan, D. L., et al. 2013, PASA, 30, 31

Datta, A., Bowman, J. D., & Carilli, C. L. 2010, ApJ, 724, 526

Di Matteo, T., Perna, R., Abel, T., & Rees, M. J. 2002, ApJ, 564, 576

Dillon, J. S., Liu, A., & Tegmark, M. 2013, Phys. Rev. D, 87, 043005

Dillon, J. S., Liu, A., Williams, C. L., et al. 2014, Phys. Rev. D, 89, 023002

Furlanetto, S. R., & Briggs, F. H. 2004, New A Rev., 48, 1039

Furlanetto, S. R., Oh, S. P., & Briggs, F. H. 2006, Phys. Rep., 433, 181

Ghosh, A., Prasad, J., Bharadwaj, S., Ali, S. S., & Chengalur, J. N. 2012, MNRAS, 426, 3295

Gleser, L., Nusser, A., & Benson, A. J. 2008, MNRAS, 391, 383

Iliev, I. T., Shapiro, P. R., Ferrara, A., & Martel, H. 2002, ApJ, 572, L123

Liu, A., Parsons, A. R., & Trott, C. M. 2014a, Phys. Rev. D, 90, 023018

—. 2014b, Phys. Rev. D, 90, 023019

Liu, A., & Tegmark, M. 2011, Phys. Rev. D, 83, 103006

Liu, A., Tegmark, M., Bowman, J., Hewitt, J., & Zaldarriaga, M. 2009, MNRAS, 398, 401

Lonsdale, C. J., Cappallo, R. J., Morales, M. F., et al. 2009, IEEE Proceedings, 97, 1497

Madau, P., Meiksin, A., & Rees, M. J. 1997, ApJ, 475, 429

McQuinn, M., Zahn, O., Zaldarriaga, M., Hernquist, L., & Furlanetto, S. R. 2006, ApJ, 653, 815

Morales, M. F., Bowman, J. D., & Hewitt, J. N. 2006, ApJ, 648, 767

Morales, M. F., Hazelton, B., Sullivan, I., & Beardsley, A. 2012, ApJ, 752, 137

Morales, M. F., & Hewitt, J. 2004, ApJ, 615, 7

Neben, A. R., Bradley, R. F., Hewitt, J. N., et al. 2015, ArXiv e-prints, arXiv:1505.07114

Paciga, G., Albert, J. G., Bandura, K., et al. 2013, MNRAS, 433, 639

Parsons, A. R., Pober, J. C., Aguirre, J. E., et al. 2012, ApJ, 756, 165

Parsons, A. R., Backer, D. C., Foster, G. S., et al. 2010, AJ, 139, 1468

Pober, J. C., Parsons, A. R., Aguirre, J. E., et al. 2013, ApJ, 768, L36

Santos, M. G., Cooray, A., & Knox, L. 2005, ApJ, 625, 575

Scott, D., & Rees, M. J. 1990, MNRAS, 247, 510

Sunyaev, R. A., & Zeldovich, Y. B. 1972, A&A, 20, 189

Thyagarajan, N., Udaya Shankar, N., Subrahmanyan, R., et al. 2013, ApJ, 776, 6

Thyagarajan, N., Jacobs, D. C., Bowman, J. D., et al. 2015a, ApJ, 807, L28

—. 2015b, ApJ, 804, 14

Tingay, S. J., Goeke, R., Bowman, J. D., et al. 2013, PASA, 30, 7

Tozzi, P., Madau, P., Meiksin, A., & Rees, M. J. 2000, ApJ, 528, 597

Trott, C. M., Wayth, R. B., & Tingay, S. J. 2012, ApJ, 757, 101

van Haarlem, M. P., Wise, M. W., Gunst, A. W., et al. 2013, A&A, 556, A2

Vedantham, H., Udaya Shankar, N., & Subrahmanyan, R. 2012, ApJ, 745, 176

Wang, X., Tegmark, M., Santos, M. G., & Knox, L. 2006, ApJ, 650, 529

Zaldarriaga, M., Furlanetto, S. R., & Hernquist, L. 2004, ApJ, 608, 622